The B26 Cu-Zn-Ag-Au project, Brouillan volcanic complex, Abitibi greenstone belt, part 1: Geological setting and geochronology

Quentin Fayard[1,2*], Patrick Mercier-Langevin[3], Natasha Wodicka[4], Réal Daigneault[1], and Serge Perreault[2]

[1]Université du Québec à Chicoutimi, 555 Boulevard de l'Université, Chicoutimi, Quebec G7H 2B1
[2]SOQUEM Inc., 1740 Chemin Sullivan, Val-d'Or, Quebec J9P 7H1
[3]Geological Survey of Canada, 490 rue de la Couronne, Québec, Quebec G1K 9A9
[4]Geological Survey of Canada, 601 Booth Street, Ottawa, Ontario K1A 0E8
[*]Corresponding author's e-mail: quentin.fayard@gmail.com

ABSTRACT

Archean synvolcanic base metal deposits vary greatly in style and metal budget through time and space. This variability is due to contrasting geological and magmatic settings, the influence of which remains a research topic with potential exploration implications. The B26 Cu-Zn-Ag-Au project, located in the Harricana-Turgeon belt of the northern Abitibi greenstone belt, is interpreted as a volcanogenic massive sulphide deposit formed in an evolving calc-alkaline (FII-type) intermediate to felsic centre (Brouillan volcanic complex). The B26 deposit is enriched in Ag and is part of a group of precious metal-enriched Archean volcanogenic massive sulphide deposits that are associated with calc-alkaline volcanic rocks, indicating that such successions are highly prospective.

The B26 host succession, informally divided into a lower intermediate member and an upper felsic member, is composed of an andesitic base intercalated with dacitic domes, onto which the felsic member was emplaced. The felsic member comprises three geochemically and texturally distinct rhyolite units that were emplaced as sills, domes, and/or flows with associated relatively voluminous fragmental facies. This felsic succession, dated at 2728 Ma, is coeval both with the host rhyolite of the nearby Selbaie polymetallic deposit and the Brouillan pluton. It is overlain by thin sedimentary strata and cut by andesitic sills and andesitic transposed dykes. This volcanic pile, undergoing extension and containing thick permeable strata, was favourable for the development of a high-temperature hydrothermal system characterized by extensive zones of Cu-rich stringers and sub-seafloor Zn-Ag-(Pb)-rich sulphide lenses in an evolving, possibly shallow-water, active volcanic centre.

INTRODUCTION

The Archean Abitibi greenstone belt is known for its mineral wealth, including volcanogenic massive sulphide (VMS) deposits and other pre-main regional deformation (synvolcanic) polymetallic deposits (e.g. Monecke et al., 2017 and references therein). A unique concentration of Archean precious metal-rich VMS deposits is found in the Abitibi, and such provinciality suggests specific underlying genetic relationships (e.g. Mercier-Langevin et al., 2015).

Although VMS deposits are present throughout the Abitibi belt, the overall endowment varies greatly among the different volcanic assemblages. The 2734–2724 Ma Deloro assemblage (Ayer et al., 2002) contains numerous VMS deposits, including those of the Matagami, Joutel, and Chibougamau districts. It also includes the Selbaie deposit in the Brouillan volcanic complex (part of the Harricana-Turgeon belt), which hosts the Cu-Zn-Ag-Au mineralized zones of the B26 mining property (Fig. 1). The past-producing Selbaie mine (56.9 Mt at 1.85% Zn, 0.87% Cu, 39 g/t Ag, and 0.55 g/t Au: Adam, 2004) has been interpreted as an epithermal system characterized by base and precious metal veins that overprint a mostly barren massive pyrite lens (Deptuck et al., 1982; Larson, 1987; Faure et al., 1990, 1996; Larson and Hutchinson, 1993; Taner, 2000). It represents the only example of this type of ore system in the Abitibi greenstone belt. A shallow subaqueous to subaerial caldera environment of formation is inferred (Deptuck et al., 1982; Larson and Hutchinson, 1993) and the age of the epithermal-like mineralization is constrained by a crosscutting synvolcanic felsic dyke (2726 ± 3 Ma: Barrie and Krogh, 1996). The 2729 ± 4 Ma Brouillan synvolcanic pluton (Barrie and Krogh, 1996), which underlies the mineral-

Fayard, Q., Mercier-Langevin, P., Wodicka, N., Daigneault, R., and Perreault, S., 2020. The B26 Cu-Zn-Ag-Au project, Brouillan volcanic complex, Abitibi greenstone belt, part 1: Geological setting and geochronology; *in* Targeted Geoscience Initiative 5: Contributions to the Understanding of Canadian Gold Systems, (ed.) P. Mercier-Langevin, C.J.M. Lawley, and S. Castonguay; Geological Survey of Canada, Open File 8712, p. 93–107. https://doi.org/10.4095/323668

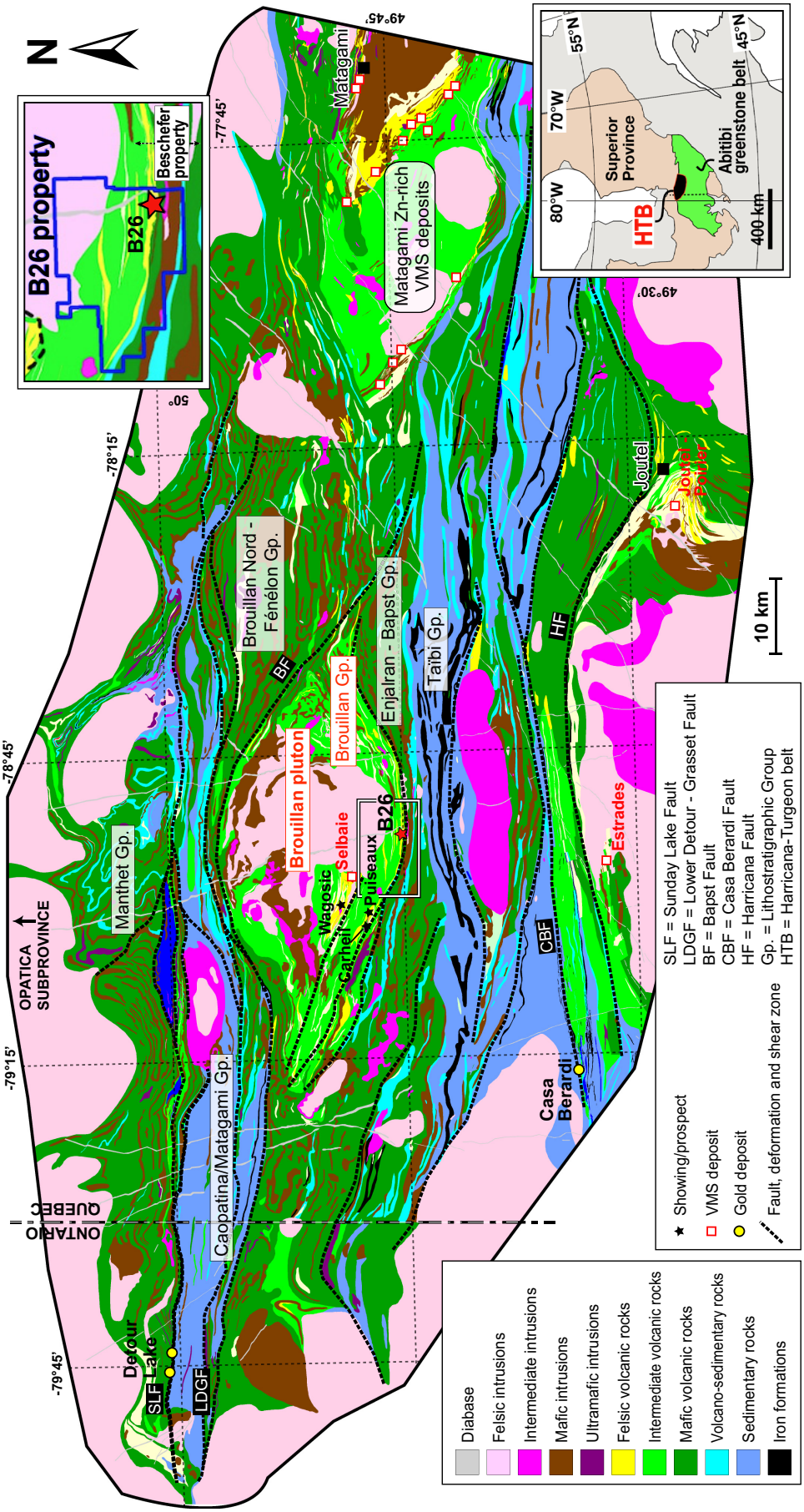

Figure 1. Regional geological map of the Harricana-Turgeon belt showing the location of the B26 project and other mineral occurrences. *Modified from* Faure (2015).

ized host succession at Selbaie, is considered as a potential driver for the hydrothermal activity associated with the base and precious metal-rich zones in the surrounding Brouillan volcanic complex (Larson and Hutchinson, 1993). One key characteristic of the Selbaie deposit is the presence of very high-grade Ag zones (i.e. up to 1–2 kg/t Ag: Taner, 2000). Such high-grade Ag intersections are also common at B26, as well as in other prospects of the area. This suggests the presence of regional controls on the precious metal-budget of some base metal deposits.

The age of the host succession at the B26 project and its potential relationship with the Selbaie deposit host rocks remain to be established. Copper-Au occurrences were discovered on the B26 property by Billiton Metals in 1997. The property was optioned in 1998 and then acquired by SOQUEM in 2009. Several drilling campaigns have been completed on the property in the last 20 years, providing a good understanding of the geological context and documentation of the B26 deposit host units (Adam, 1997; Beaudin, 2017). The "atypical" metallogenic characteristics of the Brouillan volcanic complex and the presence of locally very high Ag and Au grades (100–2000 ppm Ag, 0.5–50 ppm Au) at B26 and elsewhere in the area constitute a good opportunity to improve our understanding of precious metal enrichment processes in Archean base metal deposits.

This study is part of an M.Sc. thesis (Fayard, in prep) that aims at identifying the controls on the precious metal enrichment at B26, and this paper summarizes the geology, physical volcanology, geochemistry, and geochronology of the host volcanic succession of the B26 project. The description of the alteration and mineralized zones are presented in a companion paper (Fayard et al., 2020).

REGIONAL GEOLOGY

The Harricana-Turgeon belt in northwestern Quebec and northeastern Ontario is part of the northern Abitibi greenstone belt and extends for approximately 200 km from the Detour mine area to the Matagami district (Fig. 1). It is a volcano-sedimentary and plutonic belt mainly affected by regional greenschist-facies metamorphism, reaching the amphibolite-facies near the contact with the Opatica subprovince to the north (Lacroix, 1994). According to Lacroix et al. (1989) and Daigneault et al. (2004), the Harricana-Turgeon belt is affected by major phases of deformation, including a significant north-south shortening event (post-2710 Ma) that was responsible for the regional northwest-southeast- to east-west-trending subvertical foliation (generally referred to as S_2 at regional scale, but referred to as S_p in this study). The S_p foliation is associated with east-west-trending regional-scale folds, such as the Enjalran syncline and the Brouillan anticline. Major longitudinal faults and deformation corridors initiated during the north-south shortening were later accentuated or reactivated as dextral shears. A number of gold deposits (e.g. Detour Lake and Casa Berardi) and volcanogenic massive sulphide deposits (e.g. Matagami and Joutel districts) are present in the area (Fig. 1).

The Brouillan volcanic complex, located in the central portion of the Harricana-Turgeon belt, comprises the Brouillan Group and the Brouillan pluton. It is surrounded by the basaltic units of the Brouillan Nord-Fénélon Group to the north and Enjalran-Bapst Group to the south (Fig. 1). The Brouillan pluton is a polyphase intrusive complex composed of felsic (tonalite and granite) and intermediate (diorite) transitional to calc-alkaline phases and a mafic (gabbro) tholeiitic phase (Faure, 2012). The Brouillan Group is dominated by intermediate to felsic lapilli tuff, tuff breccia, and crystal-rich coarse tuff, intercalated with calc-alkaline to transitional andesitic flows and sills, and rhyolitic domes (Lacroix, 1994; Faure, 2012). All units dip moderately to steeply to the south (40–85º) and generally face south (Faure et al., 1996; Faure, 2012; Beaudin, 2017).

According to Lacroix (1994), Taner (2000), Beaudin (2017), and Fayard et al. (2018), strain intensity is moderate over the entire complex, except for narrow east-west-trending high-strain zones, especially in the vicinity of the Brouillan and Enjalran-Bapst contact.

The Brouillan tonalite and the Selbaie mine rhyolite have been dated at 2729 ± 4 Ma and 2729 +3/-2 Ma, respectively (Barrie and Krogh, 1996), and are considered coeval and co-magmatic. These ages were the only time constraints for the Brouillan volcanic complex prior to this study, and no age data are available for the Enjalran-Bapst Group.

MINERALIZED ZONES AT THE B26 PROJECT

The B26 mineralized system consists of stacked sulphide zones with a (transposed) discordant stringer-type Cu-rich zone at the base (Copper zone) overlain by Zn-(Pb)- and Ag-rich, concordant to stratabound, semi-massive to massive sulphide lens associated with peripheral disseminated and vein sulphides (Main and Upper Zinc zones; Fig. 2: Fayard et al., 2018). The Copper zone (indicated and inferred resources of 8.61 Mt at 1.94% Cu, 0.07% Zn, 0.97 g/t Au, and 6.84 g/t Ag: SOQUEM Inc., 2018; Camus and Valdnais-LeBlanc, 2018) consists of transposed millimetre- to decimetre-thick chalcopyrite stringers and veins that can locally contain up to 50 g/t Au. The chalcopyrite veins are associated with a large sub-concordant sericite-chlorite alteration halo and a proximal chlorite-

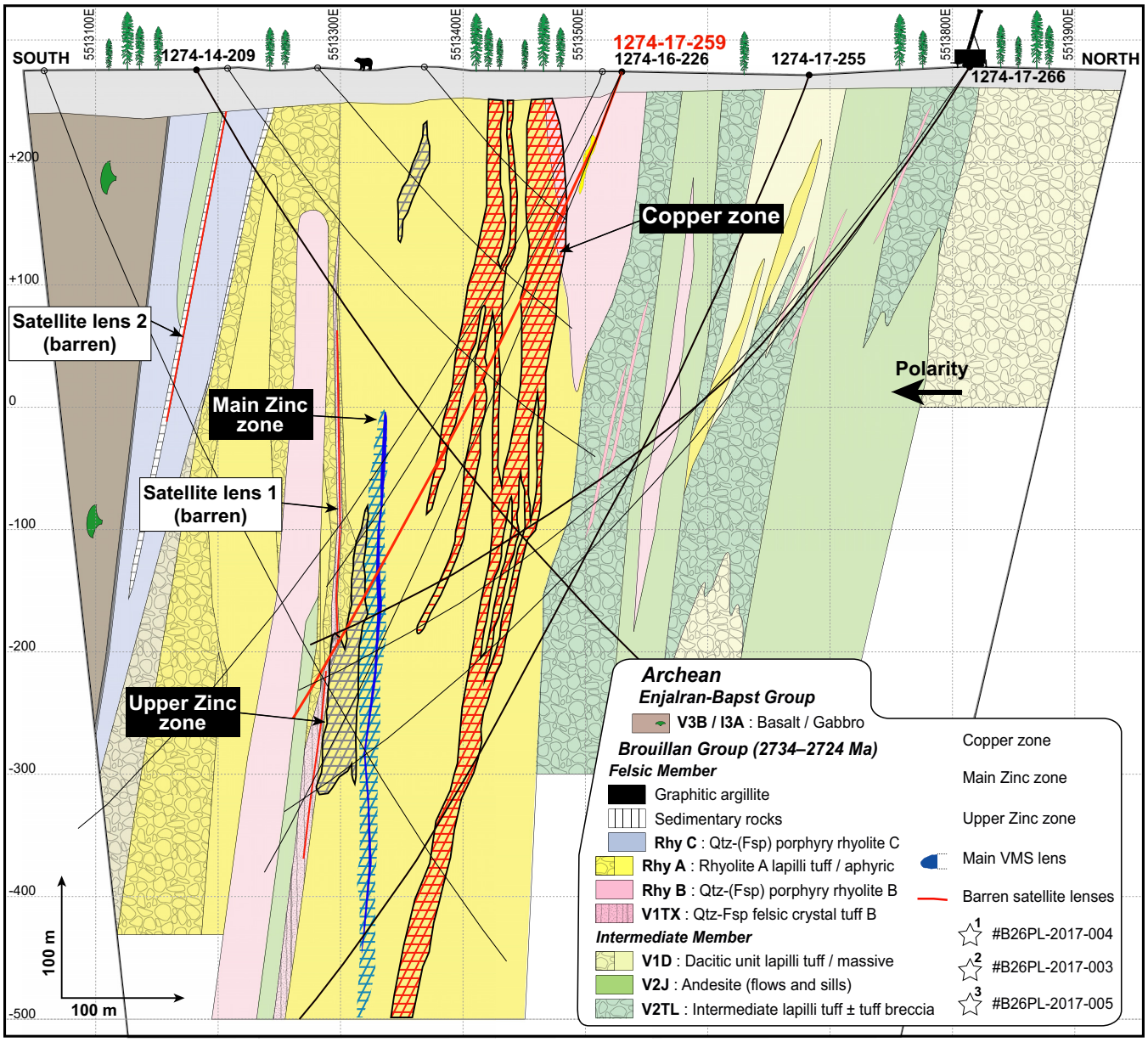

Figure 2. Simplified composite section (652950E ± 50 m) of the B26 deposit in which lithologies and mineralized zones are represented. The location (projected) of the dated U-Pb zircon geochronology samples is also shown. Abbreviations: Fsp = feldspar, Qtz = quartz.

dominated halo along the vein selvages developed in rhyolite A (*see below*). The Main and Upper Zinc zones are located in the upper part of rhyolite A (Fig. 2) and have total indicated and inferred resources of 2.77 Mt at 0.21% Cu, 4.66% Zn, 0.21 g/t Au, and 102.2 g/t Ag (SOQUEM Inc., 2018; Camus and Valdnais-LeBlanc, 2018). The Main Zinc zone consists mainly of a Zn-(Pb)-Ag semi-massive to massive sulphide lens and veins, whereas the Upper Zinc zone comprises Zn (sphalerite) disseminations, Zn-(Pb) veins, and Ag-rich (up to 2 kg/t) veins and veinlets. Mineralized zones have been metamorphosed, deformed, and transposed into the east-west-trending foliation and stretched parallel to a lineation that plunges 65°W.

VOLCANIC STRATIGRAPHY

The northwestern part of the Abitibi greenstone belt is known for its lack of outcrops, including the B26 area, which has up to a few 10s of metres of overburden. Consequently, the only available rock samples and direct observations come from drill core. In addition, most rock units are altered, deformed, and metamorphosed, which commonly hamper the recognition of protoliths and primary facies. Therefore, whole-rock lithogeochemistry was used extensively, together with the geological and petrographic drill core descriptions, to differentiate and map units at the deposit scale. From 2111 core rock samples collected from 85 drillholes, a subset of 49 least altered samples was selected to best

Table 1. Summary of the main features of the B26 deposit host volcanic rocks.

Lithology	Lithofacies	Composition and magmatic affinity	Inferred volcanic setting	Additional informations
Intermediate tuff (V2TL)	Lapilli tuff ±tuff breccia; 2–30% aphyric fragments; kilometric extent	Andesite, calc-alkaline	Autoclastic ? Pyroclastic ?	
Andesite (V2J)	Massive aphyric to locally amygdaloidal; variable thickness; kilometric extent	Andesite, calc-alkaline	Effusive (subaqueous flows), and intrusive (sills, dykes)	
Dacite (V1D)	Massive and aphyric (rare Qtz), to lapilli tuff facies; 30–120 m thick; limited extent	Dacite, calc-alkaline	Effusive, subaqueous flows and probably domes with peripheral autoclastic breccia	
Rhyolite A (Rhy A)	Massive aphyric, <3 vol.% 0.5–1.5 mm Qtz, locally relict spherulitic and flow banding textures, and lapilli tuff portions; 300 m thick; kilometric extent	Rhyolite calc-alkaline	Effusive, subaqueous flows, domes and lobes, autoclastic/talus breccia, and dykes in intermediate basement	FW: **2728.5 ± 0.8 Ma**; HW: **2727.9 ± 0.8 Ma**; Hosts Zn-Ag-(Pb) VMS lens and Cu-Au stringers; fragmental proportion probably under-estimated due to alteration/ deformation
Rhyolite B (Rhy B)	Dominant massive porphyritic facies with 10–15 vol.% of 0.5–5 mm bluish Qtz and 5–10 vol.% 0.5–5 mm Fsp (only preserved in hanging wall) in a microcrystalline matrix; minor peripheral volcaniclastic facies (Qtz-Fsp crystal-rich coarse tuff, and lapilli tuff to tuff breccia); maximum thickness 200 m in footwall and 70 m in hanging wall; kilometric extent	Rhyolite, calc-alkaline	Intrusive shallow subvolcanic sills	FW: **2728.2 ± 0.7 Ma**; The upper part of the footwall unit hosts the lower part of the Cu-Au stringers and the Qtz-Fsp crystal-rich tuff hosts the satellite barren semi-massive pyrite lens
Rhyolite C (Rhy C)	Massive porphyritic facies with 10–20 vol.% 0.5–4 mm Qtz with variable (2–10 vol.%) Fsp (usually altered); minor peripheral lapilli tuff facies; 10–50 m thick; kilometric extent	Rhyodacite/rhyolite, calc-alkaline	Intrusive as shallow subvolcanic sills and dykes (in part in the footwall), and partly effusive as flows/domes at the top of the B26 felsic member	Hosts a satellite barren massive pyrite-pyrrhotite (<1 m) lens; alternates with thin sedimentary rocks (thinly bedded argillite, siltstone, chert) and andesitic sills

Abbreviations: Fsp = feldspar, FW = footwall, HW = hanging wall, Qtz = quartz, VMS = volcanogenic massive sulphides.

characterize the initial composition of the different units present at B26. Readers are referred to Fayard (in prep) for more information about the criteria used in selecting the least altered samples.

Exploration work by Billiton Metals and SOQUEM documented six principal lithologies of the Brouillan Group at B26 (Adam, 1997; Beaudin, 2017); these lithologies have been further documented in this study: an intermediate lapilli tuff with lesser tuff breccia (V2TL), a massive andesite (V2J), a dacitic unit (V1D), an aphyric rhyolite (rhyolite A; Rhy A), a quartz- and feldspar-porphyritic rhyolite (rhyolite B; Rhy B), and a quartz±feldspar porphyritic rhyolite (rhyolite C; Rhy C; Fig. 2). The principal characteristics of these units are summarized in Table 1. Sedimentary rocks were also mapped but were not studied in detail.

The base of the host stratigraphy has only been locally intersected by drilling. It consists of a ≥500 m thick succession of andesitic to dacitic massive and volcaniclastic rocks that comprise the aforementioned intermediate lapilli tuff ± tuff breccia (V2TL), massive andesite (V2J), and dacitic unit (V1D), which are here collectively and informally referred to as the intermediate member. The mineralized zones are hosted higher in the stratigraphy in what is here informally referred to as the felsic member, which comprises rhyolite units A, B, and C. The felsic member has an approximate thickness of 400 m near the deposit (Fig. 2); the rhyolite units are intercalated with andesitic sills and dykes and minor sedimentary rocks, especially in the uppermost part. The lower intermediate member is not as well exposed as the upper felsic member because of the drilling pattern. Only a brief description of the units of the intermediate member is given here, but the rhyolite units of the felsic member are described in detail below as they host the mineralized zones and have been strongly affected by the associated hydrothermal alteration.

Intermediate Member Units

Intermediate lapilli tuff ± tuff breccia (V2TL)

This unit mostly consists of lapilli tuff with local occurrences of tuff breccia. It appears at several stratigraphic positions between the Brouillan pluton north of B26 (Fig. 1) to the base of the felsic member (Fig. 2). This

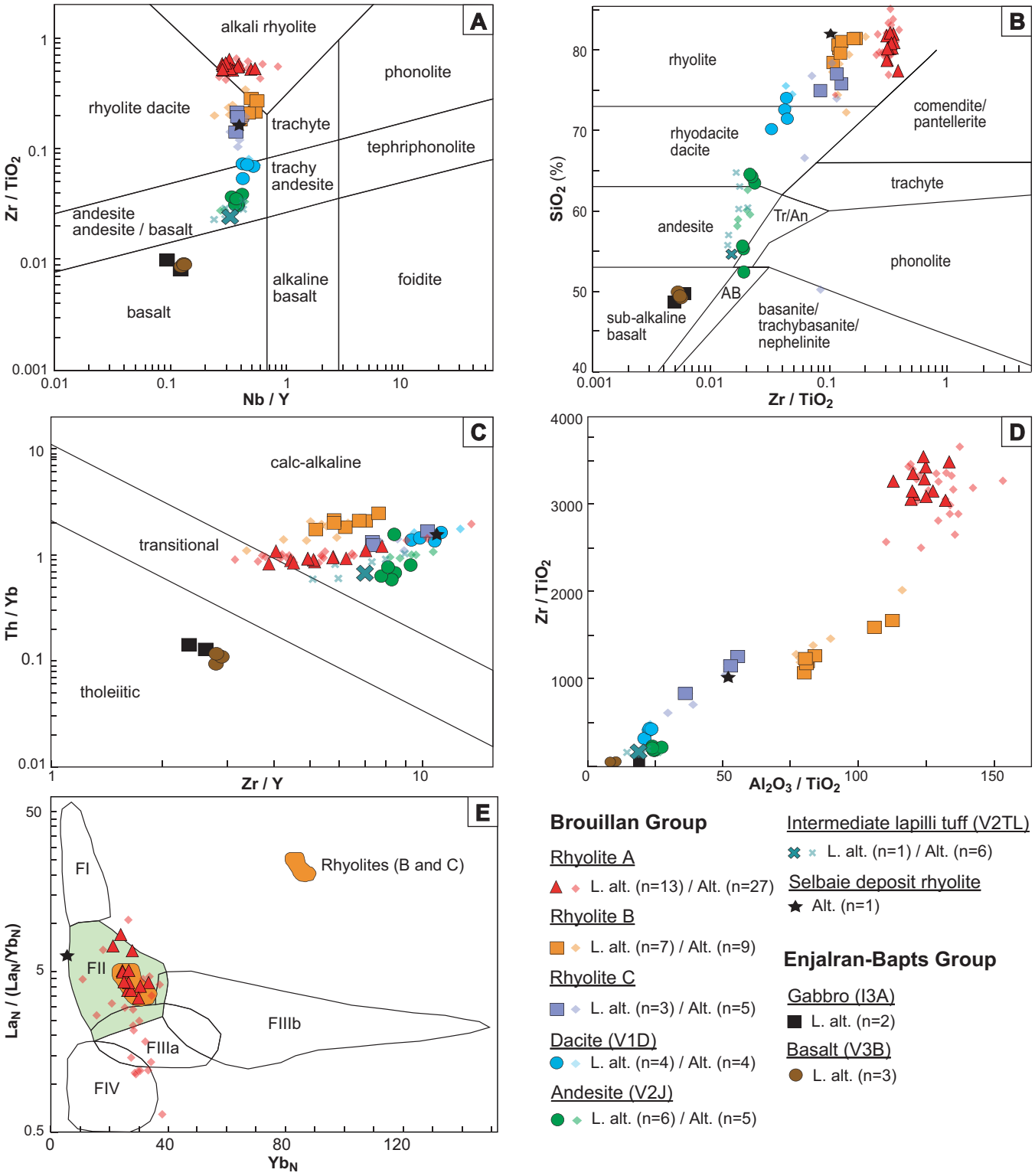

Figure 3. Diagrams illustrating the geochemical signature of the B26 volcanic rocks. **a)** (Zr ppm/10,000)/Ti (%) versus Nb/Y classification diagram of Pearce (1996). **b)** SiO_2 (%) versus (Zr ppm/10,000)/TiO_2 (%) classification diagram of Winchester and Floyd (1977). **c)** Magmatic affinity diagram of Ross and Bédard (2009). **d)** Zr/TiO_2 versus Al_2O_3/TiO_2 discrimination diagram. **e)** Rhyolite fertility diagram of Hart et al. (2004) applied to the felsic rocks only. Abbreviation: L. alt.= least altered.

unit has a basaltic-andesite to andesitic composition (Fig. 3a,b) and a calc-alkaline magmatic affinity (Fig. 3c). It is considered a fragmental facies of the andesite (V2J) unit (*see below*).

Andesite (V2J)

The andesite unit, which occurs as massive flows and sills, is a significant part of the intermediate member in the lowermost part of the stratigraphy at B26. It is also

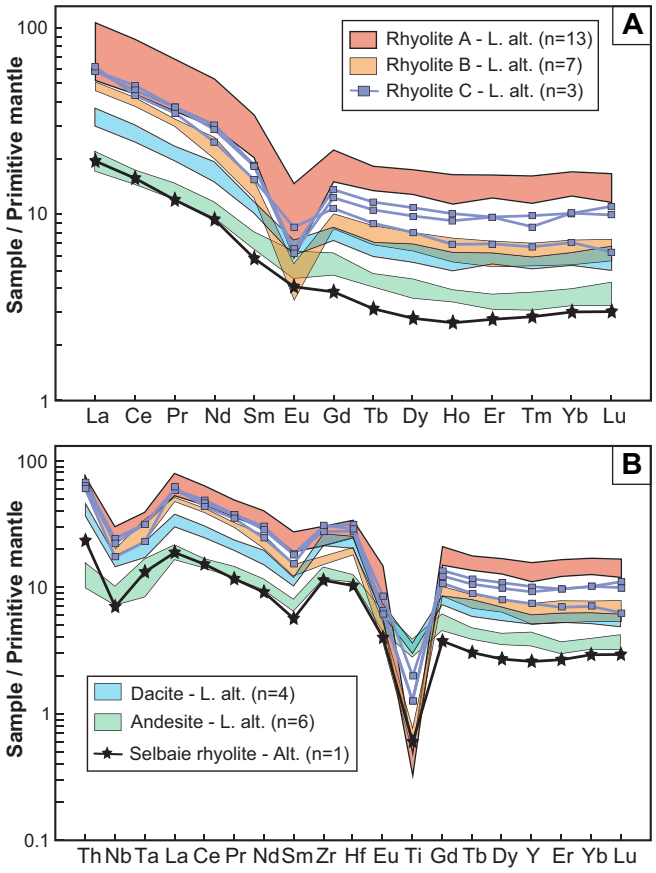

Figure 4. a) Rare earth element patterns and **(b)** multi-element patterns for the B26 host rocks. A rhyolite from Selbaie is shown for comparison. All elements are normalized to primitive mantle values of McDonough and Sun (1995).

present in the felsic member as narrow sills and thin flows in the uppermost part of the Brouillan Group stratigraphy (Fig. 2). The andesite is aphyric and has no distinctive characteristics except for some amygdales in some of the sills and uppermost flow. The composition of the andesite is andesitic with a calc-alkaline magmatic affinity (Fig. 3a,b,c). The Zr/TiO_2 and Al_2O_3/TiO_2 ratios are low at 200.9 and 24.9, respectively (Fig. 3d). The primitive mantle normalized rare earth element (REE) profile shows a moderate negative slope for the light REE ($[La/Sm]_n$ = 2.65) and an almost flat heavy REE pattern (Fig. 4a). The multi-element plot shows moderate negative Nb-(Ta) and positive Zr-Hf anomalies (Fig. 4b), typical of arc-style calc-alkaline rocks.

Dacite (V1D)

The dacite, which varies in thickness from 30 to 120 m, forms several domes with a massive core and peripheral volcaniclastic rocks (lapilli tuff and tuff breccia). The massive part is largely aphyric with a vitreous aspect but can very locally contain quartz phenocrysts (Fig. 5a). The least altered samples (n = 4) are andesitic to dacitic (Fig. 3a,b) and calc-alkaline (Fig. 3c), with relatively low Zr/TiO_2 and Al_2O_3/TiO_2 ratios at 400.8 and 22.6, respectively (Fig. 3d). The REE profile has a moderate slope for the light REEs (Fig. 4a). This unit is also characterized by moderate negative Nb-Ta and positive Zr-Hf anomalies (Fig. 4b).

Felsic Member Units

Rhyolite A (Rhy A)

Rhyolite A has a maximum thickness of 300 m in the deposit area. It hosts the Zn-mineralized zones and most of the Copper zone (Fig. 2). Although alteration and deformation hamper the recognition of primary textures in some parts of the succession, the lowermost two-thirds of the unit is dominated by massive and aphyric rocks (~70 vol.%), with local evidence of flow banding and spherulites (Fig. 5b,c). The upper third of the unit is mainly dominated by lapilli tuff (Fig. 2, 5d,e). The microcrystalline matrix of the aphyric rhyolite can locally contain 1–3 vol.% quartz phenocrysts (0.5–1.5 mm). The unit is strongly altered and deformed in the footwall of the Main and Upper Zinc zones (Fig. 5f,g). In the hanging wall, it has a slightly different, vitreous appearance (Fig. 5h). Dykes of rhyolite A are common in the intermediate member (Fig. 2).

Least altered samples (n = 13) indicate a rhyolitic composition (Fig. 3a,b). Rhyolite A is characterized by distinctly high Zr/TiO_2 and Al_2O_3/TiO_2 ratios (~3300 and ~125, respectively; Fig. 3d) due to its very low TiO_2 content (~0.08 wt%). The magmatic affinity is calc-alkaline to slightly transitional (Fig. 3c). Rhyolite A has an FII-type signature, which is typical of slightly transitional to calc-alkaline Archean rhyolite (cf. Lesher et al., 1986; Fig. 3e). The primitive mantle normalized REE profile (Fig. 4a) is characterized by a moderately negative light REE slope ($[La/Sm]_n$ = 2.74) and a flat heavy REE pattern ($[Gd/Lu]_n$ = 1.34). The entire REE pattern has a moderately negative slope ($[La/Yb]_n$ = 5.13) with a negative Eu anomaly ($[Eu/Eu^*]_n$ = 0.49). Rhyolite A is also characterized by a moderately negative Nb-Ta anomaly, a strongly negative Ti anomaly, and a very weakly positive Zr-Hf anomaly on the multi-element plot shown in Figure 4b.

Rhyolite B (Rhy B)

Rhyolite B occurs in both the footwall and hanging wall of the Main and Upper Zinc zones (Fig. 2). It forms two main masses, one at the base of rhyolite A (≤200 m thick), and the other in the uppermost part of rhyolite A (≤70 m thick; Fig. 2). Dykes and thin sills of rhyolite B also intrude the intermediate member. Rhyolite B is quartz- and feldspar-porphyritic with 10–15 vol.%, 0.5–5 mm, round to angular and commonly recrystallized (in subgrains) quartz phenocrysts in a microcrystalline quartz-feldspar matrix (Fig. 6a).

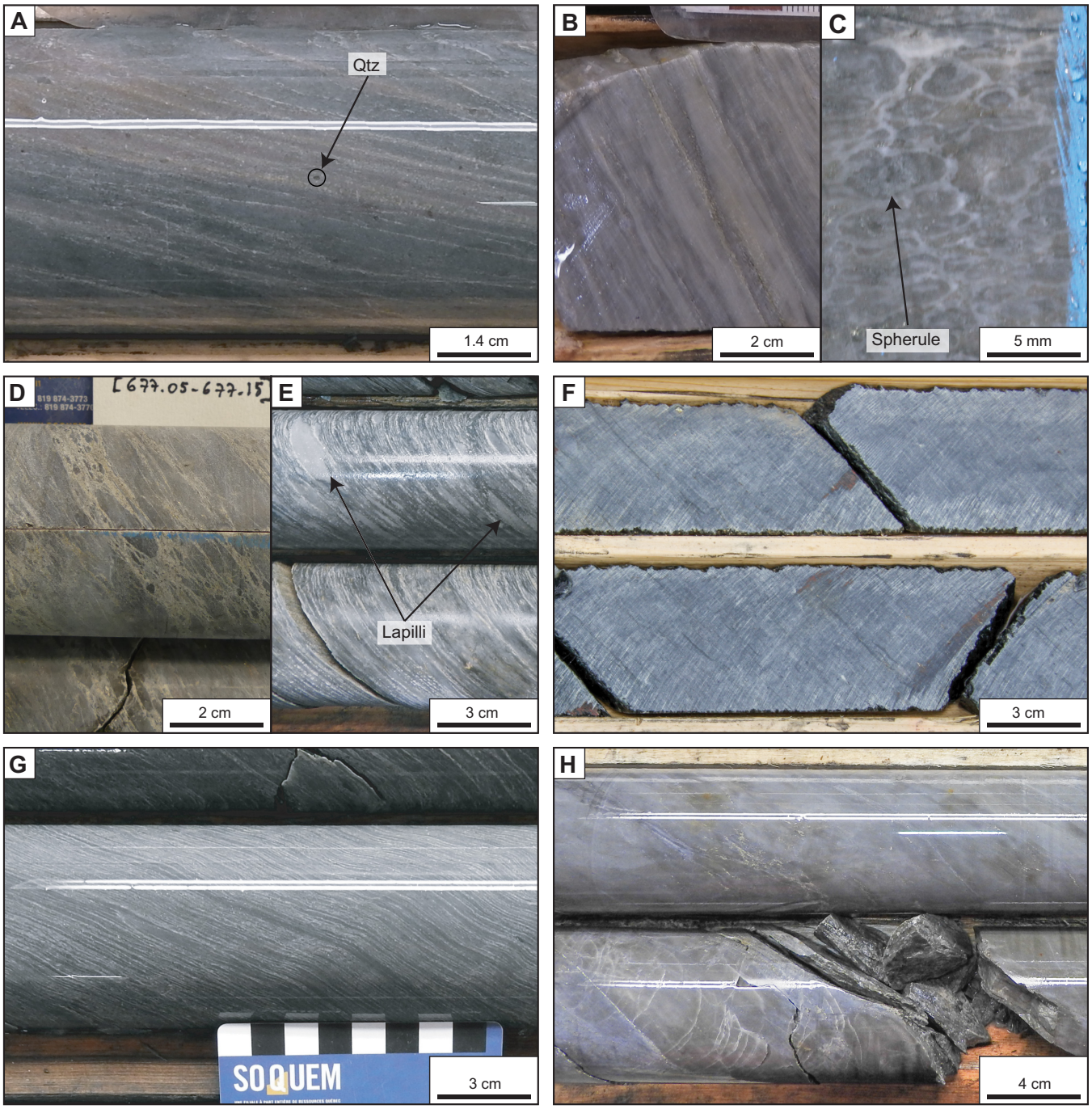

Figure 5. a) Massive dacite. **b)** Flow-banded massive aphyric rhyolite A. **c)** Spherulitic massive aphyric rhyolite A. **d-e)** Volcaniclastic facies of rhyolite A. **f)** Footwall sericite and chlorite-altered (massive) rhyolite A. **g)** Strongly foliated footwall sericite-quartz-(pyrite) altered rhyolite A. **h)** Hanging-wall aphyric and coherent rhyolite A with typical vitreous aspect. Abbreviation: Qtz = quartz.

Feldspar phenocrysts are locally preserved in the less altered hanging-wall rocks (Fig. 6b). The unit is massive for the most part (≥90 vol.%) with a minor proportion of volcaniclastic rocks including coarse tuff, lapilli tuff, and rare tuff breccia. The coarse, 2 to 4 m thick tuff bed is present in the lowermost part of the rhyolite B in the hanging wall of the Zinc zones. It contains up to 40 vol.% quartz and feldspar crystal fragments and locally some aphyric lapilli clasts (Fig. 6c,d). This tuff locally hosts a barren semi-massive pyrite lens (satellite lens 1; Fig. 2). The lapilli tuff and rare tuff breccia (Fig. 6e) are present along the margins of rhyolite B masses and can be up to a few metres thick.

Least altered samples (n = 7) indicate that rhyolite B is rhyodacitic to rhyolitic (Fig. 3a,b) and calc-alkaline (Fig. 3c) with an FII-type signature (Fig. 3e). There are some variations in the Zr/TiO_2 and Al_2O_3/TiO_2 ratios (Fig. 3d). Moderate negative slope of light REEs

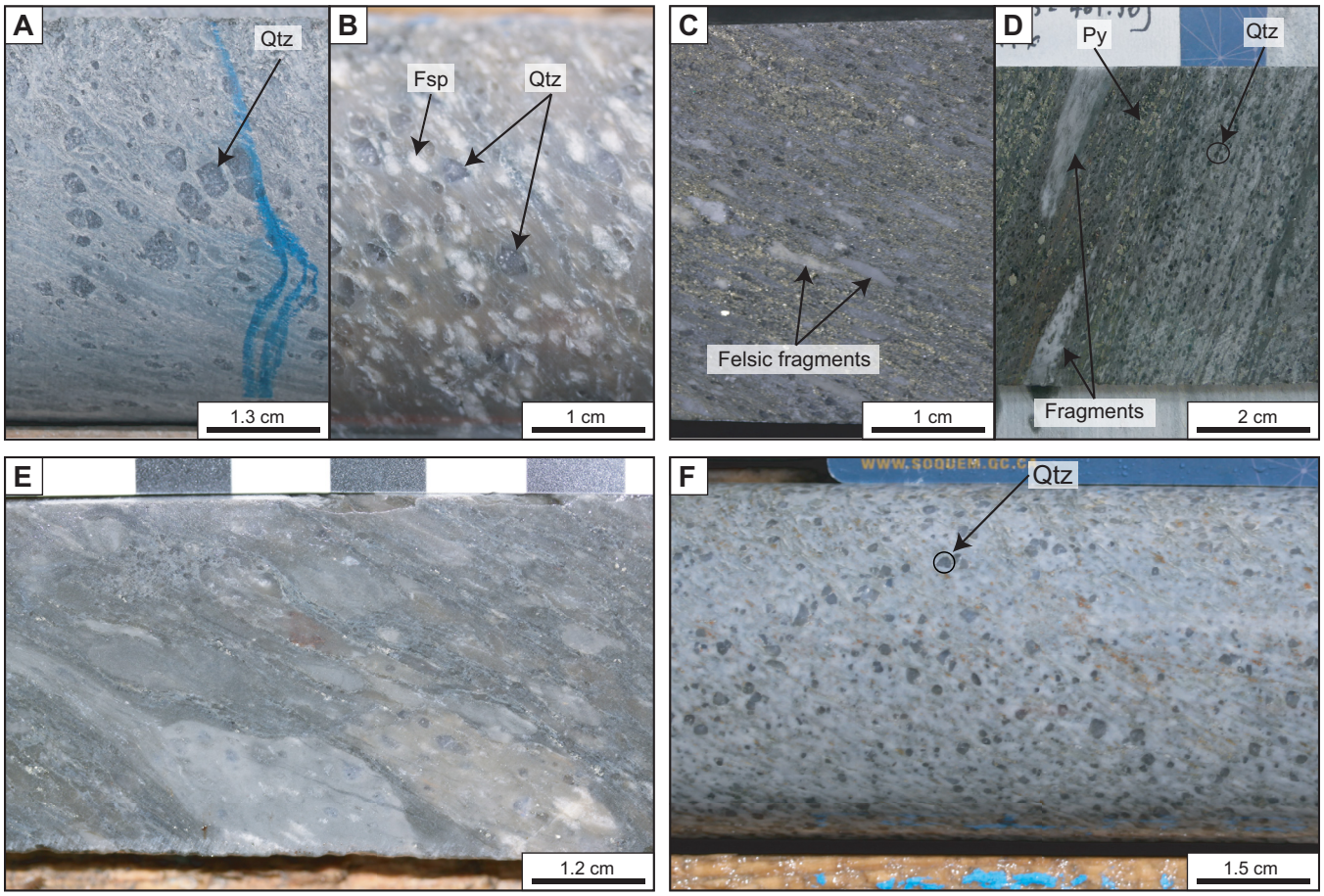

Figure 6. a) Footwall sericite and chlorite-altered quartz porphyritic rhyolite B. **b)** Hanging-wall quartz- and feldspar-phyric rhyolite B. **c)** Quartz and feldspar crystal-bearing coarse tuff facies of the hanging-wall rhyolite B. **d)** Lapilli tuff facies of the hanging-wall rhyolite B. **e)** Fragmental facies (lapilli tuff) of rhyolite B. **f)** Quartz-(feldspar) porphyritic rhyolite C. Abbreviations: Fsp = feldspar, Py = pyrite, Qtz = quartz.

($[La/Sm]_n = 3.37$), an almost flat heavy REE ($[Gd/Lu]_n = 1.42$) pattern, and a strong negative Eu anomaly ($[Eu/Eu^*]_n = 0.36$) characterize this unit (Fig. 4a). Rhyolite B is also characterized by negative anomalies in Nb-Ta and Ti (Fig. 4b).

Rhyolite C (Rhy C)

Rhyolite C is a 10 to 50 m thick, mostly massive unit that occurs in the uppermost part of the B26 host sequence (Fig. 2). It is spatially associated with andesitic sills. The unit stratigraphically overlies rhyolite A and the contact is locally brecciated. It is very locally associated with ankerite-altered sandstone and argillite hosting a 0.5 to 1 m thick barren pyrite-pyrrhotite semi-massive lens (satellite lens 2; Fig. 2).

Rhyolite C comprises 10–20 vol.% subangular to subrounded quartz phenocrysts (0.5–4 mm; Fig. 6f). The phenocrysts are commonly recrystallized in subgrains and have a bluish colour. Feldspar is rarely preserved and has undergone selective sericite alteration and stretching.

Least altered samples (n = 3) indicate a rhyodacitic to rhyolitic composition (Fig. 3a,b). Rhyolite C is geochemically distinguished from the other B26 rhyolites by its lower SiO_2 content and its relatively higher Zr, TiO_2, Al_2O_3, and Hf contents (Fayard, in prep). It is calc-alkaline (Fig. 3c) and shows a similar, but slightly more enriched heavy REE pattern compared to rhyolite B (Fig. 4a). Rhyolite C is differentiated from rhyolite units A and B by its positive Zr-Hf anomaly and a less developed negative anomaly in Ti (Fig. 4b).

Sedimentary Rocks

Sedimentary rocks gradually evolve, up-stratigraphy, from thinly bedded ±cherty siltstone to argillite. They overlie rhyolite A and are interlayered with rhyolite C and andesitic rocks at the top of the felsic member, close to the contact with the Enjalran-Bapst Group (Fig. 2).

Enjalran-Bapst Group Mafic Rocks

The Enjalran-Bapst Group is separated from the Brouillan Group (felsic member) by a thin graphitic argillite layer. The Enjalran-Bapst Group is composed of aphyric basalt and fine- to coarse-grained gabbro. These rocks have a basaltic composition (Fig. 3a,b) and

a tholeiitic affinity (Fig. 3c) that strongly contrasts with the calc-alkaline affinity of the Brouillan Group rocks. In the B26 project area, the regional deformation does not affect the Enjalran-Bapst rocks as much as the underlying Brouillan Group rocks. Fayard (in prep) provides more information about the relationship between the Enjalran-Bapst and Brouillan groups.

U-Pb ZIRCON GEOCHRONOLOGY

To better constrain the timing of formation of the B26 mineralized zones and to establish correlations with other ore deposits of the region, a series of three drill core samples from the felsic member was selected for U-Pb zircon geochronology. Two of the samples analyzed were from the Main Zinc zone footwall succession (samples B26PL-2017-003 and B26PL-2017-004 from rhyolite units A and B, respectively) and one from the hanging wall (B26PL-2017-005 from rhyolite A). Analysis was completed at the Geochronology Laboratory of the Geological Survey of Canada in Ottawa. Heavy minerals were concentrated from the samples using standard crushing, grinding, and separation on a Wilfley table and by heavy liquid techniques. Mineral separates were sorted by magnetic susceptibility using a FrantzTM isodynamic separator and hand-picked using a binocular microscope. Single zircon grains were chemically abraded following the techniques of Mattinson (2005), including annealing for 48 hours at 1000°C prior to leaching with hydrofluoric acid (HF) at 180°C for 12 hours. Details of zircon morphology, quality, and HF leaching times are summarized in Table 2. U-Pb isotope dilution-thermal ionization mass spectrometry (ID-TIMS) techniques utilized in this study—including the addition of a ^{205}Pb-^{233}U-^{235}U spike—dissolution, column chemistry, and analysis on a Triton thermal ionization mass spectrometer, are modified after Parrish et al. (1987). The treatment of analytical errors follows Roddick (1987), with regression analysis modified after York (1969). Procedural blank levels were generally less than 1.0 pg for Pb. U-Pb ID-TIMS analytical results are presented in Table 2 and displayed in concordia plots in Figure 7). All age uncertainties and error ellipses are presented at the 2σ level. The zircon grains that were analyzed were mostly euhedral to subhedral, equant to prismatic, and ranged in length from 50 to 150 µm. The three rhyolite samples, B26PL-003, -004, and -005, yielded concordant to slightly discordant analyses with similar weighted average ^{207}Pb/^{206}Pb ages of 2728.5 ± 0.8 Ma, 2728.2 ± 0.7 Ma, and 2727.9 ± 0.8 Ma, respectively, which are interpreted as the crystallization ages of the rhyolite units (Fig. 7).

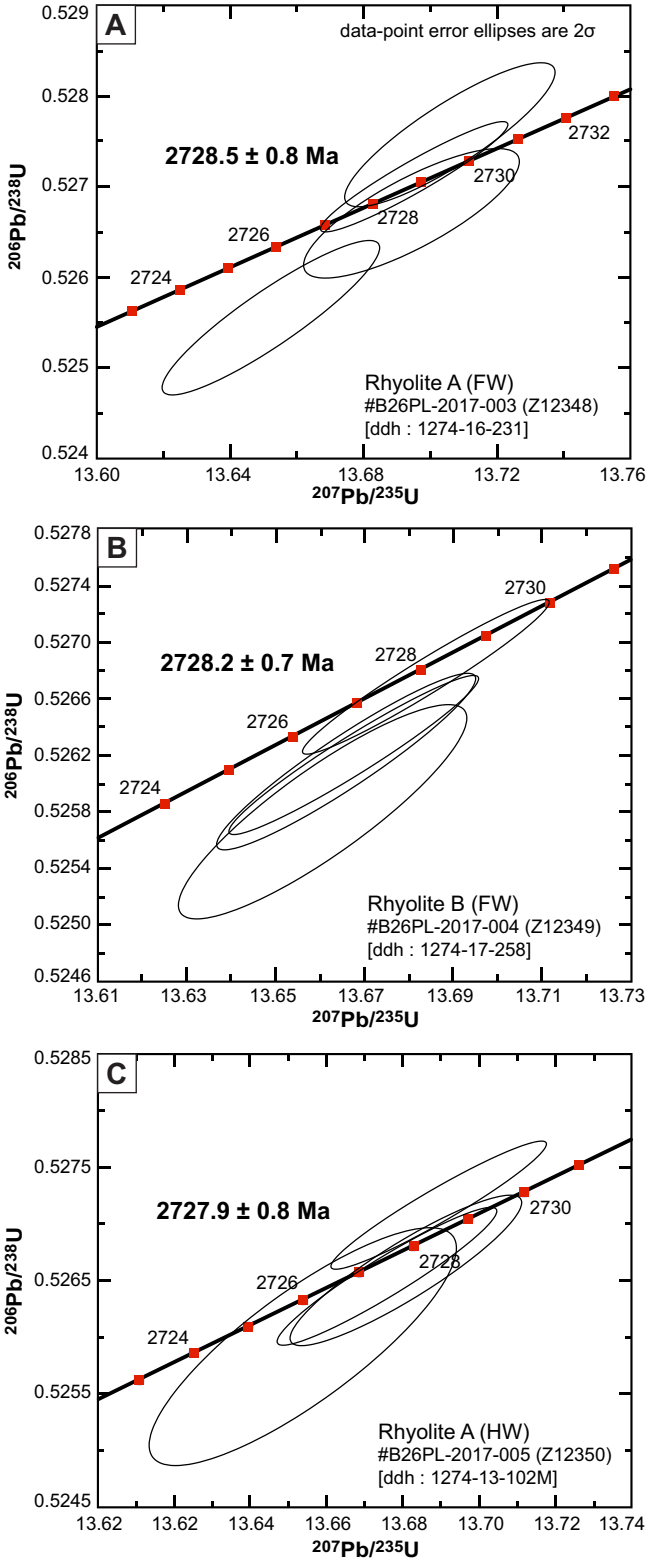

Figure 7. Concordia plots of U-Pb isotope dilution-thermal ionization mass spectrometry (ID-TIMS) analyses for the three dated samples. **a)** Footwall rhyolite A. **b)** Footwall rhyolite B. **c)** Hanging-wall rhyolite A. Error ellipses at 2σ. Abbreviations: ddh = diamond drillhole; FW = footwall; HW = hanging wall.

Table 2. U-Pb isotope dilution-thermal ionization mass spectrometry (ID-TIMS) analytical data from the host rhyolite units A and B of the B26 mineralized zones.

		Composition					Isotopic Ratios										Dates (Ma)						
Fraction[§]	Description[*]	Wt[a] (µg)	U (ppm)	$\frac{Th^b}{U}$	$\frac{Pb^{*c}}{Pb^d}$ (pg)	Pb[cd] (pg)	$\frac{Pb^{*e}}{Pb^c}$	$\frac{^{206}Pb^f}{^{204}Pb}$	$\frac{^{208}Pb^g}{^{206}Pb}$	$\frac{^{207}Pb^g}{^{235}U}$	±2σ (%)	$\frac{^{206}Pb^g}{^{238}U}$	±2σ (%)	Corr.[h] coeff.	$\frac{^{207}Pb^g}{^{206}Pb}$	±2σ (%)	$\frac{^{207}Pb^i}{^{235}U}$	±2σ (abs)	$\frac{^{206}Pb^i}{^{238}U}$	±2σ (abs)	$\frac{^{207}Pb^i}{^{206}Pb}$	±2σ (abs)	%[j] Disc.
B26PL-2017-003 (Rhyolite A): Z12348																							
A12-1 (1)	Co,Clr,Su,Pr,CA12	2.9	40	0.60	71	0.85	83.8	4494	0.16	13.650	0.201	0.52552	0.13574	0.905	0.18838	0.09186	2725.7	1.9	2722.6	3.0	2728.1	1.6	0.2
A12-2 (1)	Co,Clr,Su,Eq,rIn,CA12	3.3	37	0.57	74	1.82	40.8	2210	0.16	13.694	0.199	0.52670	0.11362	0.800	0.18856	0.12330	2728.7	1.9	2727.5	2.5	2729.6	2.1	0.1
A12-3 (1)	Co,Clr,Eu,Pr,rFr,CA12	2.6	52	0.63	84	0.42	198.5	10546	0.17	13.694	0.173	0.52711	0.09642	0.945	0.18842	0.08179	2728.8	1.6	2729.3	2.1	2728.4	1.4	0.0
A12-4 (1)	Co,Clr,Su,St,rFr,CA12	2.6	17	0.40	26	0.44	59.8	3347	0.11	13.705	0.194	0.52759	0.12565	0.866	0.18841	0.10081	2729.6	1.8	2731.3	2.8	2728.3	1.7	-0.1
B26PL-2017-004 (Rhyolite B): Z12349																							
A12-1 (1)	Co,Clr,Su,Pr,Frag,rIn,CA12	4.7	20	0.58	58	0.99	58.7	3170	0.16	13.660	0.194	0.52580	0.11949	0.873	0.18843	0.10220	2726.4	1.8	2723.7	2.7	2728.5	1.8	0.2
A12-2 (1)	Co,Clr,Eu,Pr,fFr,rIn,CA12	17	31	0.54	315	0.50	628.0	33957	0.15	13.684	0.166	0.52677	0.08587	0.966	0.18840	0.07992	2728.1	1.6	2727.8	1.9	2728.3	1.4	0.0
A12-3 (1)	Co,Clr,Su,Pr,fFr,rIn,CA12	4.2	35	0.38	87	0.46	189.9	10627	0.11	13.666	0.174	0.52616	0.09851	0.939	0.18837	0.08256	2726.8	1.7	2725.2	2.2	2728.0	1.5	0.1
A12-4 (1)	Co,Clr,Su,Pr,fFr,rIn,CA12	7.6	38	0.59	178	0.54	329.9	17685	0.16	13.667	0.168	0.52620	0.08883	0.960	0.18838	0.08042	2726.9	1.6	2725.4	2.0	2728.1	1.4	0.1
B26PL-2017-004 (Rhyolite A): Z12350																							
A12-1 (1)	Co,Clr,Su,Pr,rFr,CA12	1.2	40	0.63	29	0.54	54.2	2894	0.17	13.653	0.242	0.52591	0.16554	0.829	0.18829	0.13575	2726.0	2.3	2724.2	3.7	2727.3	2.3	0.1
A12-2 (1)	Co,Clr,Su,Pr,fFr,CA12	4.3	51	0.61	136	0.53	255.4	13628	0.17	13.676	0.172	0.52654	0.09566	0.945	0.18837	0.08132	2727.5	1.6	2726.9	2.1	2728.0	1.4	0.0
A12-3 (1)	Co,Clr,Su,Pr,Frag,fFr,rIn,CA12	1.8	43	0.55	47	0.59	80.0	4329	0.15	13.680	0.182	0.52659	0.10470	0.902	0.18842	0.09273	2727.8	1.7	2727.1	2.3	2728.4	1.6	0.0
A12-4 (1)	Co,Clr,Su,Pr,fFr,CA12	5.9	46	0.61	168	0.78	215.2	11478	0.17	13.689	0.169	0.52717	0.08907	0.954	0.18833	0.08191	2728.4	1.6	2729.5	2.0	2727.6	1.5	-0.1

Notes:

§ Number in bracket refers to the number of zircon grains in the analysis.

* Fraction descriptions: CA12 = chemically abraded for 12 hours, Clr = clear, Co = colourless, El = elongate, Eq = equant, Eu = euhedral, fFr = few fractures, Frag = fragment, In = inclusions, Pr = prismatic, rFr = rare fractures, rIn = rare inclusions, St = stubby prism, Su = subhedral,

[a] Weights estimated concentration uncertainty up to 50%.

[b] Th/U ratio calculated from the $^{208}Pb/^{206}Pb$ ratio and the $^{206}Pb/^{238}U$ date of the sample.

[c] Total radiogenic Pb.

[d] Total common Pb.

[e] Ratio of radiogenic Pb (including ^{208}Pb) to common Pb.

[f] Measured ratio corrected for fractionation and spike contribution only, reduced using GSC 535 spike calibration v. 2012.

[g] Measured ratios corrected for fractionation, spike, blank, and, where applicable, initial common Pb. Laboratory blanks were corrected using $^{206}Pb/^{204}Pb = 18.20 \pm 0.47$, $^{207}Pb/^{204}Pb = 15.37 \pm 0.14$, $^{208}Pb/^{204}Pb = 37.40 \pm 0.19$.

[h] Correlation coefficient of radiogenic $^{207}Pb^*/^{235}U$ and $^{206}Pb^*/^{238}U$.

[i] Dates (Ma) calculated using $^{238}U/^{235}U = 137.88$ (Steiger and Jäger, 1977), and decay constants of $^{238}U = 1.55125 \times 10^{-10}$ yr^{-1} and $^{235}U = 9.8485 \times 10^{-10}$ yr^{-1} (Jaffey et al., 1971).

[j] % discordance = 100 - (100 * ($^{206}Pb/^{238}U$ date) / ($^{207}Pb/^{206}Pb$ date)).

DISCUSSION

Stratigraphy of the B26 Host Volcanic Succession

The inferred primary volcanic architecture of the B26 project area is schematized in Figure 8. The interpreted relative and absolute timing of the emplacement of the different units is detailed below following four phases of an evolving volcanic centre. The focus of this paper is the timing of the events and the potential architecture in the study area. Petrogenetic considerations will be presented and discussed in detail elsewhere (Fayard, in prep).

First phase: Intermediate member volcanism

The intercalated andesite and intermediate lapilli tuff ± tuff breccia deposit have the same geochemical signature, which suggests a cogenetic relationship. The relative proportion of flows versus sills is, however, difficult to estimate as both facies are texturally similar (Fig. 8). The dacite was probably coeval with the andesite as it is located at different stratigraphic positions in the andesitic strata (Fig. 8). The textures and distribution of the dacite are in agreement with an emplacement as isolated domes. These domes may have been extrusive, but they could also have been partly emplaced in a sub-seafloor setting (i.e. cryptodomes). Dacitic volcanism probably marks the gradual transition towards more felsic volcanism in the upper part of the stratigraphy. The nature of the andesite and dacite (e.g. massive with surrounding unsorted, monogenic volcaniclastic deposits) does not confirm that they were emplaced in a subaqueous setting. However, the general context strongly suggests it, although the water depth at the time of emplacement remains unconstrained.

Second phase: Early volcanism of the felsic member

The onset of calc-alkaline felsic volcanism is established at about 2728 Ma, as indicated by the two ages (2727.9 ± 0.8 and 2728.5 ± 0.8 Ma) obtained from rhyolite A. The rhyolite A was most likely emplaced as coalescing flow-dome complexes at, or very near, the seafloor, forming isolated massive, flow-foliated aphyric rhyolites in a thick pile of associated fragmental deposits (Fig. 8). Dome growth might have been in part endogenous, as suggested by the vertical continuity of some of the massive rhyolites that seem to match the dome's lateral extension. Although the age and chemistry are identical to the underlying strata, the upper third of the unit may represent a secondary pulse of rhyolite A volcanism as it has a slightly different aspect (vitreous) with more abundant volcaniclastic rocks.

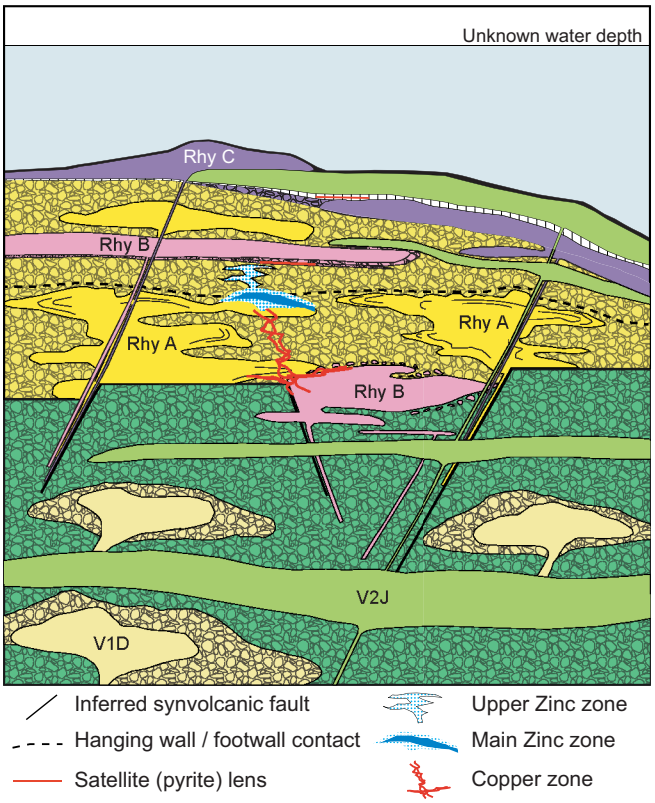

Figure 8. Schematic representation of the inferred primary architecture of the B26 host volcanic succession and the mineralized zones. Legend for the units is shown in Figure 2. Note that the colours of the volcaniclastic facies patterns have been slightly attenuated to highlight the mineralized zones.

Third phase: Rhyolite B

Volcanism related to rhyolite B is contemporaneous with that of rhyolite A as indicated by similar U-Pb crystallization ages (Fig. 7). However, both rhyolite units are distinct as indicated by their contrasting texture and slightly different chemistry. The facies and distribution of rhyolite B indicate that it was emplaced as shallow subvolcanic domes or sills at the interface between the intermediate and felsic members, and higher up in rhyolite A (Fig. 8). Such an interpretation is in agreement with the presence of common dykes and sills of rhyolite B intruding the volcanic succession.

Fourth phase: Waning volcanism and sedimentation

The age of rhyolite C is unconstrained, but its distribution and chemistry indicate that it is part of the same felsic magmatic system as the other intermediate to felsic volcanic rocks at B26. It was emplaced as a series of sills in the uppermost part of rhyolite A and extruded as flows and/or as domes on the paleo-seafloor, forming the top of the felsic member. Rhyolite C probably represents the waning stages of felsic volcanic activity

in the study area, which was succeeded by clastic sedimentation. Calc-alkaline andesitic volcanism covered the top of the volcanic edifice, forming amygdaloidal flows interlayered with rhyolite C and sediments. Finally, a thin layer of graphitic argillite covers the entire volcanic sequence.

Geological Controls on the Style and Geometry of Mineralized Zones

The volcanic architecture in the B26 project area comprises permeable volcaniclastic strata that were more favourable to hydrothermal fluid upflow and thus influenced the metal distribution. The transposed and slightly discordant Copper zone extends over at least 150 to 200 m of flattened stratigraphy, indicating that it was certainly significantly thicker prior to flattening. This suggests a significant vertical extension of the Cu mineralization that may have been accentuated by the permeable nature of the volcaniclastic strata. Though the Main and Upper Zinc zones are concordant, they are considered to have been formed largely by subseafloor replacement processes (*see* Fayard et al., 2020). More "diffuse-style" mineralization formed within the hanging-wall fragmental facies of rhyolite A.

The alteration is widespread and extends in the hanging-wall rocks, further supporting a sub-seafloor deposition. Although there are no constraints on the water depth at the time of volcanism, the extensive Copper zone suggests a deep setting that would have prevented fluid boiling, whereas the comparatively smaller, Pb-bearing, Ag-rich Zinc zones suggest a much lower temperature, and perhaps a shallower setting allowing fluids to boil (cf. Hannington et al., 1999). It is possible that the apparent lack of a significant hiatus (e.g. interlayered sedimentary strata) in the felsic volcanism associated with rhyolite A in the immediate B26 area could have hampered the development of a large sulphide lens. Such a hiatus seems to have only occurred during the emplacement of rhyolite C, much higher in the stratigraphy, perhaps during the waning stage or after the hydrothermal activity. This does not preclude the possibility that favourable local hiatuses in rhyolite A volcanism may have developed elsewhere in the Brouillan Group.

The volcanic succession in the Selbaie area, which occurs less than 10 km to the northwest, has the same age as that at B26. It has been interpreted as a shallow submarine to subaerial volcanic centre comprising epithermal polymetallic mineralization (e.g. Larson and Hutchinson, 1993). Thus, the B26 zones may represent an intermediate mineralization style between typical Archean Zn-Cu systems and epithermal systems. The presence of distinct intermediate to felsic units as coalescing domes and laterally restricted flows, dykes, and sills indicates that the area was undergoing extension. It also means that the area was the location of focused volcanic activity with a well developed thermal corridor (cf. Galley, 2003) in proximity to the Brouillan synvolcanic intrusion, explaining the presence of the B26 mineralized zones in that area.

Analogies between the Host Rocks of the B26 Zones and the Selbaie Deposit

The Selbaie and B26 rhyolite units are geochemically largely similar. They both have a strongly calc-alkaline magmatic affinity (Fig. 3c) and comparable extended primitive mantle-normalized trace element patterns (Fig. 4b). They have the same age (ca. 2729–2728 Ma) and are coeval with the 2729 ± 4 Ma Brouillan synvolcanic intrusion. Dissimilarities include the presence of shallow water to subaerial pyroclastic units at Selbaie, which are absent (or not preserved) at B26, perhaps explaining differences in ore styles (*see* Fayard et al., 2020 for further discussion). More work is underway to fully compare the B26 area with the Selbaie deposit.

IMPLICATIONS FOR EXPLORATION

This study presents preliminary volcanogenic, textural, geochemical, and geochronological information about the B26 Cu-Zn-Ag-Au project, which provides a better understanding of the key stratigraphic relationships between the volcanic units and the mineralization, and how these relate to the large past-producing Selbaie polymetallic deposit. B26 is a base metal (Zn-Cu) polymetallic mineralized system that contains significant Ag-rich zones. It is hosted in a ≥400 m thick sequence of predominantly felsic flows, domes, and sills that have a calc-alkaline magmatic affinity. It is also located very proximal to a large synvolcanic felsic calc-alkaline intrusion (Brouillan pluton), which is interpreted to have been the hydrothermal driver in the area (e.g. Selbaie deposit and Wagosic prospect). Archean calc-alkaline volcanic centres have traditionally been considered less prospective than tholeiitic successions. However, B26, Selbaie, and the Ag-rich mineralized zones of the Brouillan volcanic complex are similar to many of the Archean Au-rich VMS systems of the Superior province (e.g. Mercier-Langevin et al., 2015). They are associated with calc-alkaline rocks, indicating that such rocks (typical of very well metal-endowed younger arc settings) should not be neglected in exploring for Archean synvolcanic ore systems.

ACKNOWLEDGMENTS

This report is a contribution to the Targeted Geoscience Initiative Program of the Geological Survey of Canada. Support for this study was provided through the Gold Project, Activity G-1.1: Gold through space and time at

the Archean. Quentin Fayard is conducting a TGI-supported M.Sc. at the Université du Québec à Chicoutimi. The authors would like to thank SOQUEM Inc. for their support and collaboration in this study and access to data. Zircon mineral separates were prepared by R. Chung and G. Case at the Geological Survey of Canada. P. Hunt oversaw zircon imaging for in-situ SHRIMP analyses. SHRIMP data acquisition and data reduction were conducted with the help of T. Pestaj and N. Rayner. This report benefited from constructive comments by P-S. Ross and S. Castonguay.

REFERENCES

Adam, D., 1997. Rapport d'une campagne de forage, propriété B26, canton Brouillan, Québec, Canada; Les métaux Billiton Canada Inc., GM 57187, 14 p.

Adam, D., 2004. Les Mines Selbaie, final ore reserves statement as of January 22, 2004; Unpublished internal report to BHP Billiton, 25 p.

Ayer, J.A., Amelin, Y., Corfu, F., Kamo, S., Ketchum, J., Kwok, K., and Trowell, N., 2002. Evolution of the southern Abitibi greenstone belt based on U-Pb geochronology: autochthonous volcanic construction followed by plutonism, regional deformation and sedimentation; Precambrian Research, v. 115, p. 63–95.

Barrie, C.T. and Krogh, T.E., 1996. U-Pb zircon geochronology of the Selbaie Cu-Zn-Ag-Au mine, Abitibi Subprovince, Canada; Economic Geology, v. 91, p. 563–575.

Beaudin, A., 2017. Rapport de la campagne de sondages hiver-été 2014, propriété B26, canton Brouillan, Québec, Canada; SOQUEM Inc., GM 70058, 45p.

Camus, Y. and Valdnais-Leblanc, O., 2018. Rapport Technique NI 43-101 et estimation des ressources, Projet B26, Québec; Unpublished internal report to Soquem Inc, 136 p.

Daigneault, R., Mueller, W.U., and Chown, E.H., 2004. Abitibi greenstone belt plate tectonics: the diachronous history of arc development, accretion and collision; *in* The Precambrian Earth: Tempos and events, (ed.) P.G. Eriksson, W. Altermann, D.R. Nelson, W.U. Mueller, and O. Catuneanu; Developments in Precambrian Research, v. 12, p. 88–103.

Deptuck, R., Squair, H., and Wierzbicki, V., 1982. Geology of the Detour zinc-copper deposits, Brouillan Township, Quebec; *in* Precambrian sulfide deposits, H.S. Robinson Memorial Volume, (ed.) R.W. Hutchinson, C.D. Spence, and J.M. Franklin; Geological Association of Canada, Special Paper 25, p. 319–342.

Faure, S., Jébrak, M., and Bouillon, J.J., 1990. Géologie et minéralisations en Zn–Cu–Ag–Au de Les Mines Selbaie; *in* The northwestern Quebec polymetallic belt; a summary of 60 years of mining exploration. Proceedings of the Rouyn-Noranda 1990 symposium, (ed.) M. Rive, P. Verpaelst, Y. Gagnon, J.M. Lulin, G. Riverin, and A. Simard; Canadian Institute of Mining and Metallurgy, Special Volume 43, p. 363–372.

Faure, S., Jébrak, M., and Angelier, J., 1996. Structural evolution of Les Mines Selbaie, northern Abitibi, Québec, Canada; Exploration and Mining Geology, v. 5, p. 215–230.

Faure, S., 2012. Réévaluation paléo environnementale du complexe volcanique de Selbaie et de son potentiel métallogénique; CONSOREM project 2011-08, 26 p. <http://www.consorem.ca/production_scientifique/2011_08/Rapport%202011-08%20Selbaie.pdf> [accessed November 15, 2019]

Faure, S., 2015. Prolongement de la faille Sunday Lake (mine Detour Gold, Ont.) au Québec et son potentiel pour les minéralisations aurifères et en métaux de base; CONSOREM Project 2013-02, 41 p. < http://www.consorem.ca/production_scientifique/2013_02/Rapport%202013-02%20DETOUR_VF_20160401.pdf> [accessed November 15, 2019]

Fayard, Q., Mercier-Langevin, P., Daigneault, R., and Perreault, S., 2018. Volcanic, hydrothermal and structural controls on the nature and distribution of base and precious metals at the B26 project, Brouillan volcanic complex, Abitibi, Quebec; *in* Targeted Geoscience Initiative: 2017 report of activities, volume 1, (ed.) N. Rogers; Geological Survey of Canada, Open File 8358, p. 99–103.

Fayard, Q., Mercier-Langevin, P., Daigneault, R., and Perreault, S., 2020. The B26 Cu-Zn-Ag-Au project, Brouillan volcanic complex, Abitibi greenstone belt, part 2: Hydrothermal alteration and mineralization; *in* Targeted Geoscience Initiative 5: Contributions to the Understanding of Canadian Gold Systems, (ed.) P. Mercier-Langevin, C.J.M. Lawley, and S. Castonguay; Geological Survey of Canada, Open File 8712, p. 109–125. doi:10.4095/323669

Galley, A.G., 2003. Composite synvolcanic intrusions associated with Precambrian VMS-related hydrothermal systems; Mineralium Deposita, v. 38, p. 443–473.

Hannington, M.D., Poulsen, H.K., Thompson, J.F.H., and Sillitoe, R.H., 1999. Volcanogenic gold in the massive sulfide environment; *in* Volcanic-associated massive sulfide deposits: processes and examples in modern and ancient settings, (ed.) C.T. Barrie and M.D. Hannington; Reviews in Economic Geology, v. 8, p. 325–356.

Hart, T.R., Gibson, H. L., and Lesher, C.M., 2004. Trace element geochemistry and petrogenesis of felsic volcanic rocks associated with volcanogenic massive Cu-Zn-Pb sulfide deposits; Economic Geology, v. 99, p. 1003–1013.

Jaffey, A.H., Flynn, K.F., Glendenin, L.E., Bentley, W.C., and Essling, A.M., 1971. Precision measurements of half-lives and specific activities of ^{235}U and ^{238}U; Physical Review, v. 4, p. 1889–1906.

Lacroix, S., Simard, A., Pilote, P., and Dubé, L. M., 1989. Vers une image régionale du sillon Harricana-Turgeon (Matagami-Joutel-Casa-Berardi); Ministère de l'Énergie et des Ressources du Québec, PRO 89-04, 7 p.

Lacroix, S., 1994. Géologie de la partie ouest du sillon Harricana-Turgeon, Abitibi; Ministère des Ressources naturelles du Québec, MB 94-54, 26 p.

Larson, J.E., 1987. Geology, geochemistry and volcanic history of Les Mines Selbaie, Quebec, Canada: An Archean epithermal system; Ph.D. thesis, Colorado School Mines, Boulder, Colorado, 388 p.

Larson, J.E. and Hutchinson, R.W., 1993. The Selbaie Zn-Cu-Ag deposits, Quebec, Canada; an example of evolution from subaqueous to subaerial volcanism and mineralization in an Archean caldera environment; Economic Geology, v. 88, p. 1460–1482.

Lesher, C.M., Goodwin, A.M., Campbell, I.H., and Gorton, M.P., 1986. Trace-element geochemistry of ore-associated and barren, felsic metavolcanic rocks in the Superior province, Canada; Canadian Journal of Earth Sciences, v. 23, p. 222–237.

Mattinson, J.M., 2005. Zircon U–Pb chemical abrasion ("CA-TIMS") method; combined annealing and multi-step partial dissolution analysis for improved precision and accuracy of zircon ages; Chemical Geology, v. 220, p. 47–66.

McDonough, W.F. and Sun S-S., 1995. The composition of the Earth; Chemical Geology, v. 120, p. 223–253.

Mercier-Langevin, P., Hannington, M.D., Dubé, B., Piercey, S.J., Peter, J.M., and Pehrsson, S.J., 2015. Precious metal enrichment processes in volcanogenic massive sulphide deposits – a summary of key features, with an emphasis on TGI-4 research

contributions; *in* Targeted Geoscience Initiative 4: Contributions to the understanding of volcanogenic massive sulphide deposits genesis and exploration methods development, (ed.) J.M. Peter and P. Mercier-Langevin; Geological Survey of Canada Open File 7853, p. 117–130.

Monecke, T., Mercier-Langevin, P., Dubé, B., and Friemen, B., 2017. Geology of the Abitibi greenstone belt; *in* Archean base and precious metal deposits, southern Abitibi greenstone belt, Canada, (ed.) T. Monecke, P. Mercier-Langevin, and B. Dubé; Reviews in Economic Geology, v. 19, p. 7–49.

Parrish, R.R., Roddick, J.C., Loveridge, W.D., and Sullivan, R.W., 1987. Uranium-lead analytical techniques at the Geochronology Laboratory; Geological Survey of Canada, Paper 87-2, p. 3–7.

Pearce, J.A., 1996. A user's guide to basalt discrimination diagrams; *in* Trace Element Geochemistry of Volcanic Rocks: Applications for massive sulphide exploration, (ed.) D.A. Wyman, Geological Association of Canada, Short Course notes 12, p. 79–113.

Roddick, J.C., 1987. Generalized numerical error analysis with applications to geochronology and thermodynamics; Geochimica et Cosmochimica Acta, v. 51, p. 2129–2135.

Ross, P.-S. and Bédard, J.H., 2009. Magmatic affinity of modern and ancient subalkaline volcanic rocks determined from trace element discriminant diagrams; Canadian Journal of Earth Sciences, v. 46, p. 823–839.

SOQUEM Inc., 2018. SOQUEM divulgue une nouvelle estimation des ressources du gîte B26; Press release, 6 p. <https:// www.soquem.qc.ca/wp-content/uploads/com_soquem_fr_4_ mars_ final.pdf> [accessed November 15, 2019]

Steiger, R.H. and Jagger, E., 1977. Subcommission on geochronology: Convention on the use of decay constants in geo- and cosmochronology; Earth and Planetary Science Letters, v. 36, p. 359–362.

Taner, M.F., 2000. The Geology of the volcanic-associated polymetallic (Zn, Cu, Ag and Au) Selbaie deposits, Abitibi, Quebec, Canada; Exploration and Mining Geology, v. 9, p. 189–214.

Winchester, J.A. and Floyd, P.A., 1977. Geochemical discrimination of different magma series and their differentiation products using immobile elements; Chemical Geology, v. 20, p. 325–343.

York, D., 1969. Least squares fitting of a straight line with correlated errors; Earth and Planetary Science Letters, v. 5, p. 320–324.